



| | |
|--------------|--|
| Title | Local pressure components and interfacial tensions of a liquid film in the vicinity of a solid surface with a nanometer-scale slit pore obtained by the perturbative method |
| Author(s) | Fujiwara, K.; Shibahara, M. |
| Citation | Journal of Chemical Physics. 2015, 142(9), p. 094702 |
| Version Type | VoR |
| URL | https://hdl.handle.net/11094/93597 |
| rights | This article may be downloaded for personal use only. Any other use requires prior permission of the author and AIP Publishing. This article appeared in Fujiwara K., Shibahara M.. Local pressure components and interfacial tensions of a liquid film in the vicinity of a solid surface with a nanometer-scale slit pore obtained by the perturbative method. Journal of Chemical Physics. 7 March 2015; 142, 094702, and may be found at https://doi.org/10.1063/1.4913495 . |
| Note | |

The University of Osaka Institutional Knowledge Archive : OUKA

<https://ir.library.osaka-u.ac.jp/>

The University of Osaka

Local pressure components and interfacial tensions of a liquid film in the vicinity of a solid surface with a nanometer-scale slit pore obtained by the perturbative method

K. Fujiwara and M. Shibahara

Citation: *The Journal of Chemical Physics* **142**, 094702 (2015); doi: 10.1063/1.4913495

View online: <http://dx.doi.org/10.1063/1.4913495>

View Table of Contents: <http://scitation.aip.org/content/aip/journal/jcp/142/9?ver=pdfcov>

Published by the [AIP Publishing](#)

Articles you may be interested in

[A novel weighted density functional theory for adsorption, fluid-solid interfacial tension, and disjoining properties of simple liquid films on planar solid surfaces](#)

J. Chem. Phys. **131**, 024704 (2009); 10.1063/1.3174928

[Finite system size effects in the interfacial dynamics of binary liquid films](#)

J. Chem. Phys. **129**, 044701 (2008); 10.1063/1.2953440

[Liquids confined in wedge shaped pores: Nonuniform pressure induced by pore geometry](#)

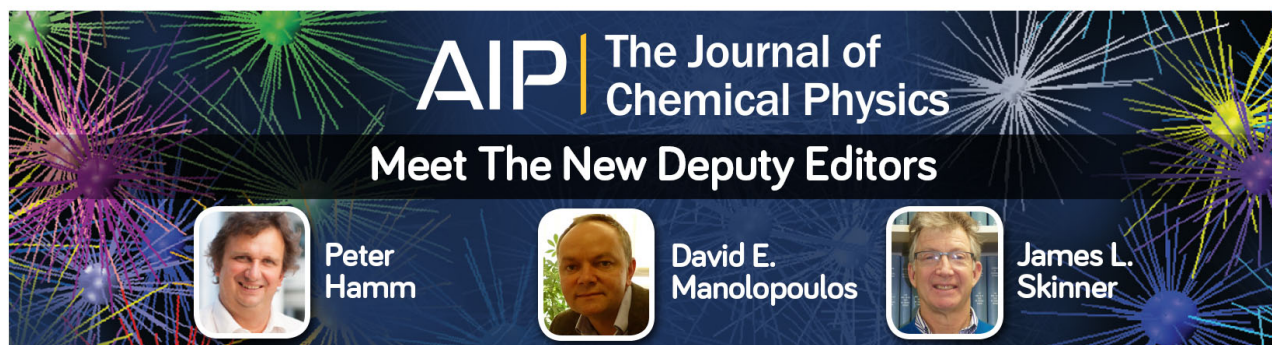
J. Chem. Phys. **120**, 11355 (2004); 10.1063/1.1764771

[Physical model for the evaluation of solid-liquid interfacial tension in silicon](#)

J. Appl. Phys. **90**, 750 (2001); 10.1063/1.1379349

[Application of density functional perturbation theory to pure fluid liquid-vapor interfaces](#)

J. Chem. Phys. **113**, 2447 (2000); 10.1063/1.482062



AIP | The Journal of
Chemical Physics

Meet The New Deputy Editors

| | | | | | |
|---|-------------------|---|------------------------------|---|-------------------------|
|  | Peter Hamm |  | David E. Manolopoulos |  | James L. Skinner |
|---|-------------------|---|------------------------------|---|-------------------------|

Local pressure components and interfacial tensions of a liquid film in the vicinity of a solid surface with a nanometer-scale slit pore obtained by the perturbative method

K. Fujiwara^{1,2,a)} and M. Shibahara^{2,b)}

¹*R & D Department, SCREEN Holdings Co., Ltd., 322 Furukawa-cho, Hazukashi, Fushimi-ku, Kyoto, Kyoto 612-8486, Japan*

²*Department of Mechanical Engineering, Graduate School of Engineering, Osaka University, 2-1 Yamadaoka, Suita, Osaka 565-0871, Japan*

(Received 26 October 2014; accepted 12 February 2015; published online 2 March 2015)

A classical molecular dynamics simulation was conducted for a liquid-solid interfacial system with a nanometer-scale slit pore in order to reveal local thermodynamic states: local pressure components and interfacial tensions of a liquid film in the vicinity of the slit. The simulation also examined the transition mechanism between the two states of the liquid film: (a) liquid film on the slit and (b) liquid film in the slit, based on the local thermodynamic quantities from a molecular point of view. An instantaneous expression of the local pressure components and interfacial tensions, which is based on a volume perturbation, was presented to investigate time-dependent phenomena in molecular dynamics simulations. The interactions between the particles were described by the 12-6 Lennard-Jones potential, and effects of the fluid-solid interaction intensity on the local pressure components and interfacial tensions of the fluid in the vicinity of the slit were examined in detail by the presented perturbative method. The results revealed that the local pressure components tangential to the solid surface in the vicinity of the 1st fluid layer from the solid surface are different in a two dimensional plane, and the difference became pronounced in the vicinity of the corner of the slit, for cases where the fluid-solid interaction intensities are relatively strong. The results for the local interfacial tensions of the fluid inside the slit suggested that the local interfacial tensions in the vicinity of the 2nd and 3rd layers of the solid atoms from the entrance of the slit act as a trigger for the transition between the two states under the influence of a varying fluid-solid interaction. © 2015 AIP Publishing LLC. [<http://dx.doi.org/10.1063/1.4913495>]

I. INTRODUCTION

A liquid-solid interface, where the solid surface has nanometer-scale structures, allows room to study not only complicated systems which are directly related to the real world, for instance, systems which consist of polymer molecules interacting with solid surfaces having terminations which produce quantum effects, but also simple systems consisting of molecules such as spherical particles interacting by the Lennard-Jones (LJ) potential. However, phenomena at a structured liquid-solid interface, such as evaporation, condensation, diffusion, and wetting, are related to complex physics and chemistry over a wide range of temporal-spatial scale, and hence, it is difficult to obtain a complete picture of the phenomena.^{1,2} In the semiconductor industry, with the help of the photolithographic technique which enables us to produce nanometer-scale structures,³ controlling those phenomena in the vicinity of the structures is a crucial issue especially in the wet cleaning process used to manufacture semiconductor devices,⁴ and a precise understanding of those phenomena is also beneficial to design surfaces to control the mass, momentum, and energy transport phenomena which occur at and through the interface.

The state of a structured liquid-solid interface can be classified into the two situations shown in Fig. 1, where we consider an ideal model of a liquid film in the vicinity of a solid surface with a slit pore.

These two states are historically called Cassie-Baxter⁵ and Wenzel⁶ states if the shape of the liquid on the solid surface is a droplet, and the difference between the states plays an important role in controlling the phenomena at the structured liquid-solid interface. In recent years, the two states are intensively investigated in the progress in superhydrophobic surface developments,⁷⁻⁹ and the results of the molecular simulations show that the fluid-solid interaction intensity has a dominant influence on the relationship between the two states, in relation to the wetting phenomena.¹⁰⁻¹⁵ However, under the influence of a varying fluid-solid interaction, the local thermodynamic state of the liquid in the vicinity of the solid surface having nanometer-scale structures, which is intimately involved in the interfacial phenomena, and the transition mechanism between the two states based on the local thermodynamic quantities have yet to be revealed in detail from a molecular point of view.

The intensive variable, pressure, one of the fundamental thermodynamic quantities and directly connected to the interfacial tension, is indispensable for discussion of such interfacial phenomenon, and its microscopic expressions derived by Irving and Kirkwood,¹⁶ and Todd *et al.*¹⁷ are applied in

^{a)}Electronic mail: ku.fujiwara@screen.co.jp

^{b)}Electronic mail: siba@mech.eng.osaka-u.ac.jp

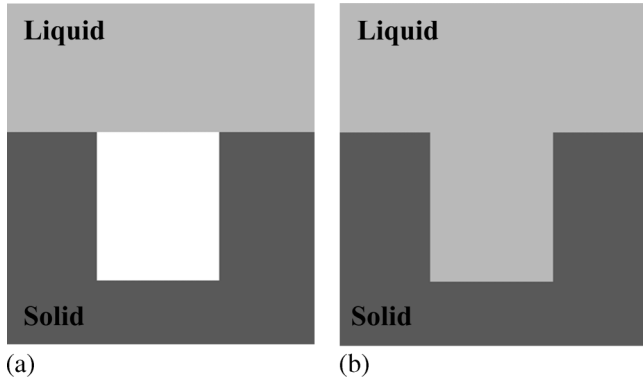


FIG. 1. Schematic illustration of the two states of the liquid-solid interface with a slit pore. (a) Liquid film on the slit pore. (b) Liquid film in the slit pore.

molecular simulations. On the other hand, the pressure and interfacial tension are defined by using the partition function for each ensemble based on statistical thermodynamics,¹⁸ and the expressions are effectively used by the perturbative methods such as Volume perturbation (VP) and Test area (TA) methods intensively developed by de Miguel and Jackson,¹⁹ Ghoufi *et al.*^{20–22} and Gloor *et al.*²³ Recently, Fujiwara and Shibahara²⁴ proposed a general description of the perturbative method to obtain the local pressure components and interfacial tension at a fluid-solid interface for a system in the canonical and grand canonical ensembles, which interacts with an external field, and showed its effectiveness by the molecular dynamics method. However, the system consisted of flat interfaces, and the method was applicable only to an equilibrium state.

In the present paper, a liquid-solid interfacial system with a nanometer-scale slit pore was investigated by the classical molecular dynamics simulation in order to reveal local thermodynamic states: local pressure components and interfacial tensions of a liquid film in the vicinity of the slit. The simulation also provides information on the transition mechanism between the two states of the liquid film: (a) liquid film on the slit and (b) liquid film in the slit, based on the local thermodynamic quantities from a molecular point of view. In order to investigate time-dependent phenomena by molecular dynamics simulations, a volume perturbation method is presented which can obtain instantaneous values of the local pressure components and interfacial tensions. The interactions between fluid-fluid, solid-solid, and fluid-solid particles are described by the 12-6 Lennard-Jones potential, and effects of the fluid-solid interaction intensity on the local pressure components and interfacial tensions of the fluid in the vicinity of the slit are examined in detail by the presented perturbative method.

This paper is organized as follows. Section II gives a method to obtain the local pressure components and interfacial tensions, which is based on a volume perturbation for a system which interacts with an external field. Section III describes detailed numerical conditions and the system used in the present study: a liquid-solid interfacial system with a slit pore. The results of the pressure components of the liquid film on or in the slit are shown in Sec. IV, and effects of the local interfacial tensions in the vicinity of the slit on the two states of

the liquid film are investigated. The conclusions of this study are summarized in Sec. V.

II. AN EXPRESSION OF INSTANTANEOUS PRESSURE COMPONENTS AND INTERFACIAL TENSIONS BY A VOLUME PERTURBATION

As described in Sec. I, the established perturbative method based on the statistical thermodynamics is applicable in an equilibrium system; therefore, instantaneous values cannot be obtained by the method. However, the nature of the perturbative method: the evaluation of the potential energy through the volume perturbation, can be used as a technique of the molecular dynamics simulation for investigations of time-dependent phenomena. In this section, an instantaneous expression of the local pressure components and interfacial tensions is proposed by using a volume perturbation, and the relationship between the established equation applicable in equilibrium and the instantaneous expression is discussed in Appendix A.

Consider a fluid-solid interfacial system consisting of the local volume $V_k (= dx_k \times dy_k \times dz_k)$ and $V = \sum_k V_k$ in which fluid particles are interacting with solid atoms as an external field. Based on the instantaneous expression of the pressure,^{17,24} the $\xi (= x, y, \text{ or } z)$ component of the instantaneous pressure, acting on a plane A_{ξ, V_k} which is perpendicular to ξ coordinate in the local volume V_k , $\hat{P}_{\xi\xi, V_k}$ is expressed as

$$\hat{P}_{\xi\xi}(x, y, z) \equiv \hat{P}_{\xi\xi, V_k} = \frac{1}{V_k} \sum_{i \in V_k} \frac{p_{i\xi}^2}{m_i} + \frac{1}{A_{\xi, V_k}} (f_{\xi} + f'_{\xi}), \quad (1)$$

where $p_{i\xi}$ and m_i are ξ component of the momentum and mass of the i th particle, respectively. f_{ξ} is the total ξ component of the intermolecular force between fluid particles acting on the local plane A_{ξ, V_k} in V_k , and f'_{ξ} is the total ξ component of the intermolecular force acting on the fluid particles due to the interactions with solid particles, through the local plane A_{ξ, V_k} in V_k . The value of the hydrodynamic velocity is assumed to be small, and is ignored in Eq. (1). The first and second terms on the right hand side in Eq. (1) represent the volume-averaged expression of the kinetic part of the particles and the intermolecular forces acting on a plane, respectively. The second term on the right hand side in Eq. (1) is expressed as the numerical evaluation of the force acting on a plane as below,

$$\frac{1}{A_{\xi, V_k}} (f_{\xi} + f'_{\xi}) = -\frac{\Delta(U_{V_k} + \Phi_{V_k})}{\Delta(d\xi_k)A_{\xi, V_k}}, \quad (2)$$

where $\Delta(d\xi_k) = \lambda d\xi_k$, and λ is the perturbation parameter which has a small value in simulations. U_{V_k} is the potential energy in V_k between the fluid particles, and Φ_{V_k} is the potential energy in V_k contributed by the external field. These potential energies in V_k are evaluated by considering only the interactions through the local plane A_{ξ, V_k} . The method to obtain the local energies in the molecular dynamics simulation is presented in detail in Appendix B. Considering Eq. (2), the instantaneous pressure component $\hat{P}_{\xi\xi, V_k}$ becomes, as a

volume-perturbed expression,

$$\hat{P}_{\xi\xi,V_k} = \frac{1}{\Delta(d\xi_k)A_{\xi,V_k}} \left[\sum_{i \in V_k} \frac{p_{i\xi}^2}{m_i} \frac{\Delta V_k}{V_k} - \Delta(U_{V_k} + \Phi_{V_k}) \right]. \quad (3)$$

Here, ΔV_k denotes a small volume perturbation in the ξ direction, and defined as $\Delta V_k = \Delta(d\xi_k)A_{\xi,V_k}$. Equation (3) indicates that evaluations of the momentum of fluid particles in the local volume V_k , and of the variations of the potential energies U_{V_k} and Φ_{V_k} through the volume perturbation, are needed to obtain the instantaneous pressure component $\hat{P}_{\xi\xi,V_k}$.

From Eq. (3), the local interfacial tension is defined in the present study as²⁴

$$\hat{\gamma}_{\xi-\eta}(x, y, z) \equiv \hat{\gamma}_{\xi-\eta,V_k} = (\hat{P}_{\xi\xi,V_k} - \hat{P}_{\eta\eta,V_k}) d\xi_k, \quad (4)$$

$(x, y, z) \in V_k$

where normal and tangential directions to an interface are described as ξ and η , respectively. Equation (4) is based on the formula,^{25,26}

$$\gamma = \int (P_{\xi} - P_{\eta}) d\xi, \quad (5)$$

which is defined in an equilibrium state. Therefore, the quantity defined in Eq. (4) means a part consisting of the interfacial tension related to a macroscopic concept. The local interfacial tension can be obtained by the molecular dynamics simulations considering the contribution of the energy to the local volume (see Appendix B).

The difference of the energy U_{V_k} in Eq. (3) is evaluated as follows, as described in detail in Refs. 19–24. For instance, \hat{P}_{zz,V_k} is calculated by the volume variation of the system from the initial state of $V_{k,0} = dx_{k,0} \times dy_{k,0} \times dz_{k,0}$ to the perturbed state of $V_{k,1} = dx_{k,1} \times dy_{k,1} \times dz_{k,1}$, where $dz_{k,1} = dz_{k,0}(1 + \lambda)$ with the perturbation parameter λ , keeping the values of $dx_{k,1}$ and $dy_{k,1}$ constant: $dx_{k,1} = dx_{k,0}$ and $dy_{k,1} = dy_{k,0}$. The relative positions of the fluid particles to the solid particles should be considered for the evaluation of Φ_{V_k} in Eq. (3), due to the fact that the volume of the system is defined as the region of fluid particles.²⁴ Consider a fluid-solid interfacial system with a slit pore as shown in Fig. 1, where the height, width, and depth directions of the slit are defined as z , x , and y coordinates, respectively, and whose solid particles are arranged just below $z = 0.0$. The imposed conditions for the fluid-solid interfacial system with a slit pore, in the vicinity of the left side of the slit, are

$$\begin{aligned} x_{f,1} &= x_{f,0}(1 + \lambda) & \text{for } x_{f,0} > x_{s,0} & \text{and } z_{f,0} > 0, \\ x_{f,1} &= x_{f,0}(1 - \lambda) & \text{for } x_{f,0} < x_{s,0} & \text{and } z_{f,0} > 0 \end{aligned} \quad (6)$$

and

$$\begin{aligned} y_{f,1} &= y_{f,0}(1 + \lambda) & \text{for } y_{f,0} > y_{s,0} & \text{and } z_{f,0} > 0, \\ y_{f,1} &= y_{f,0}(1 - \lambda) & \text{for } y_{f,0} < y_{s,0} & \text{and } z_{f,0} > 0, \end{aligned} \quad (7)$$

where x_{fs} and y_{fs} , respectively, represent the x and y components of the distance between the fluid solid particles. The subscripts f and s indicate the values for the fluid and the solid particles, respectively. Furthermore, in the slit, the additional conditions below are needed,

$$\begin{aligned} z_{f,1} &= z_{f,0}(1 + \lambda) & \text{for } z_{f,0} > z_{s,0} & \text{and } z_{f,0} < 0, \\ z_{f,1} &= z_{f,0}(1 - \lambda) & \text{for } z_{f,0} < z_{s,0} & \text{and } z_{f,0} < 0 \end{aligned} \quad (8)$$

and

$$\begin{aligned} y_{f,1} &= y_{f,0}(1 + \lambda) & \text{for } y_{f,0} > y_{s,0} & \text{and } z_{f,0} < 0, \\ y_{f,1} &= y_{f,0}(1 - \lambda) & \text{for } y_{f,0} < y_{s,0} & \text{and } z_{f,0} < 0. \end{aligned} \quad (9)$$

III. CALCULATION SYSTEM AND NUMERICAL DETAILS

Classical molecular dynamics simulations are conducted for a system in which a liquid film exists in the vicinity of the solid surface with a slit pore as shown in Figs. 2(a) and 2(b). The liquid film exists, as the initial state either on, or in, the slit, and there is a planar solid surface at the top of the calculation system. The periodic boundary conditions are applied in the x and y directions. The number of the fluid molecules, upper, and lower solid atoms is 6300, 5670, and 12 915, respectively. All the interactions between the particles are assumed to obey the 12-6 LJ potential,

$$u(r_{ij}) = 4\epsilon \left[\left(\frac{\sigma}{r_{ij}} \right)^{12} - \left(\frac{\sigma}{r_{ij}} \right)^6 \right], \quad (10)$$

where r_{ij} is the distance between the i th and j th particles, and σ and ϵ are the constant parameters. Then, the Hamiltonian of the system of the fluid interacting with an external field is

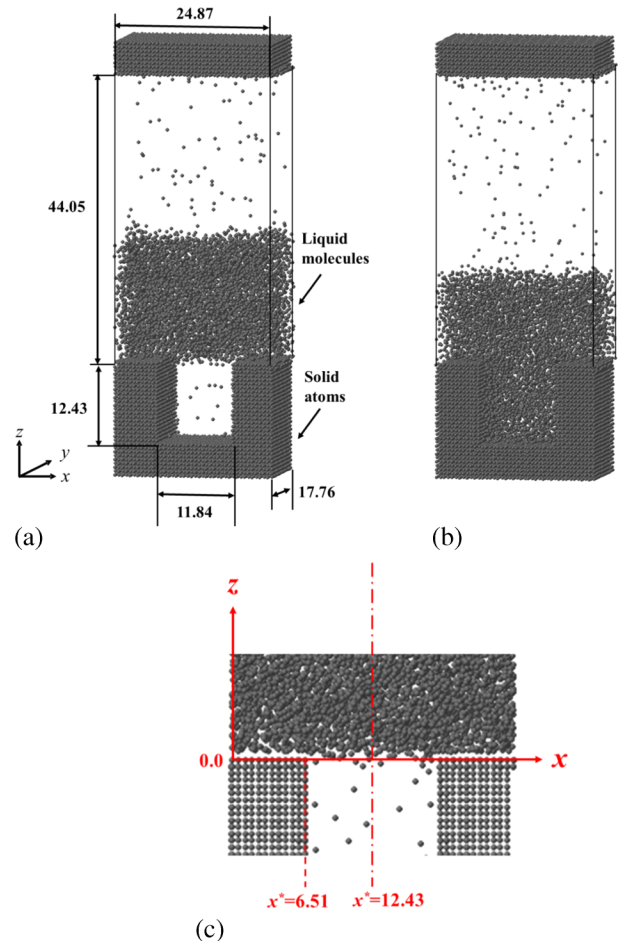


FIG. 2. Calculation systems (initial condition) and definition of the location of the coordinates. (a) Liquid film on a slit pore. (b) Liquid film in a slit pore. (c) Definition of the location of the coordinates.

described as

$$H(\mathbf{r}, \mathbf{p}) = \sum_i^{N_f} \frac{|\mathbf{p}_i|^2}{2m_f} + \frac{1}{2} \sum_{i \neq j}^{N_f} u_{ff}(r_{ij}) + u_{ext}. \quad (11)$$

In Eq. (11), \mathbf{p}_i is the momentum vector of the i th fluid molecule whose mass is described as m_f , N_f is the number of the fluid molecules, and $u_{ff}(r_{ij})$ is the potential energy between the fluid molecules. u_{ext} is defined as $u_{ext} = \sum_{i=1}^{N_f} \sum_{j=1}^{N_s} u_{fs}(r_{ij})$ with the number of the solid atoms N_s and the potential energy between the fluid molecules and the solid atoms, u_{fs} . In the present study, the fluid molecules are assumed to be argon (Ar), and reduced units are adopted by using the LJ parameters of the fluid molecules, m_f , σ_{ff} , and ε_{ff} as given in Table I. The LJ potential is truncated by using the cutoff distance, 5.0. The upper and lower solid parts are assumed to be platinum (Pt), with reduced parameters of $\sigma_{ss} = 0.746$ and $\varepsilon_{ss} = 65.39$.²⁷ For the fluid-solid interaction, the parameters of $\sigma_{fs} = (\sigma_{ff} + \sigma_{ss})/2 = 0.873$ and ε_{fs} are adopted, in which ε_{fs} is varied as a ratio to ε_{ff} . The volume above the slit, $V^u (= L_x^u \times L_y^u \times L_z^u)$ is $24.87 \times 17.76 \times 44.05$, and the volume of the slit is $11.84 \times 17.76 \times 12.43$. The definition of the coordinates in the system is illustrated in Fig. 2(c), on the zoomed figure in the vicinity of the entrance of the slit. The x^* position of the solid atoms facing the inside of the slit at the left side of the slit is 6.51, and the center of the slit is at $x^* = 12.43$. The upper and lower solid parts consist of 9 and 30 layers of the solid atoms, respectively, and the solid atoms are arrayed in a fcc lattice structure with the (111) surface in contact with the fluid part. The solid atoms in

TABLE I. Definition of the reduced units.

| Unit | Value |
|---|--|
| Mass: m_f | 6.634×10^{-26} kg |
| Distance: σ_{ff} | 3.405×10^{-10} m |
| Energy: ε_{ff} | 1.670×10^{-21} J |
| Temperature: ε_{ff}/k_B | 120.9 K |
| Time: $\sigma_{ff}(m_f/\varepsilon_{ff})^{1/2}$ | 2.146×10^{-12} s |
| Pressure: $\varepsilon_{ff}/\sigma_{ff}^3$ | 4.230×10^7 N m ⁻² |
| Interfacial tension: $\varepsilon_{ff}/\sigma_{ff}^2$ | 1.440×10^{-2} N m ⁻¹ |
| Density: m_f/σ_{ff}^3 | 1.68×10^3 kg m ⁻³ |

the 1st layers facing the fluid part can move freely around the center of oscillation by the interactions with other atoms, the temperature of the solid atoms in the 2nd layers is controlled by the Langevin method,^{28,29} at a constant value $T^* = 0.8$, and the other solid atoms are fixed. The perturbation parameter λ which is needed to evaluate the difference of the energy in Eq. (3), is chosen to have the value of 5.0×10^{-10} , and the difference is numerically evaluated by the central difference method.

The procedure to make the initial condition is as follows. First, the fluid molecules are arranged in a fcc lattice as a liquid film on the slit for a relatively weak fluid-solid interaction intensity: $\varepsilon_{fs} = 0.20$, and the temperature of the fluid molecules is kept constant by the velocity scaling control for 500 000 time steps with a time interval of $\Delta t = 9.3 \times 10^{-4}$. Second, the fluid-solid interaction intensity is changed to the target values ($0.20 < \varepsilon_{fs} < 0.50$), and the temperature is controlled

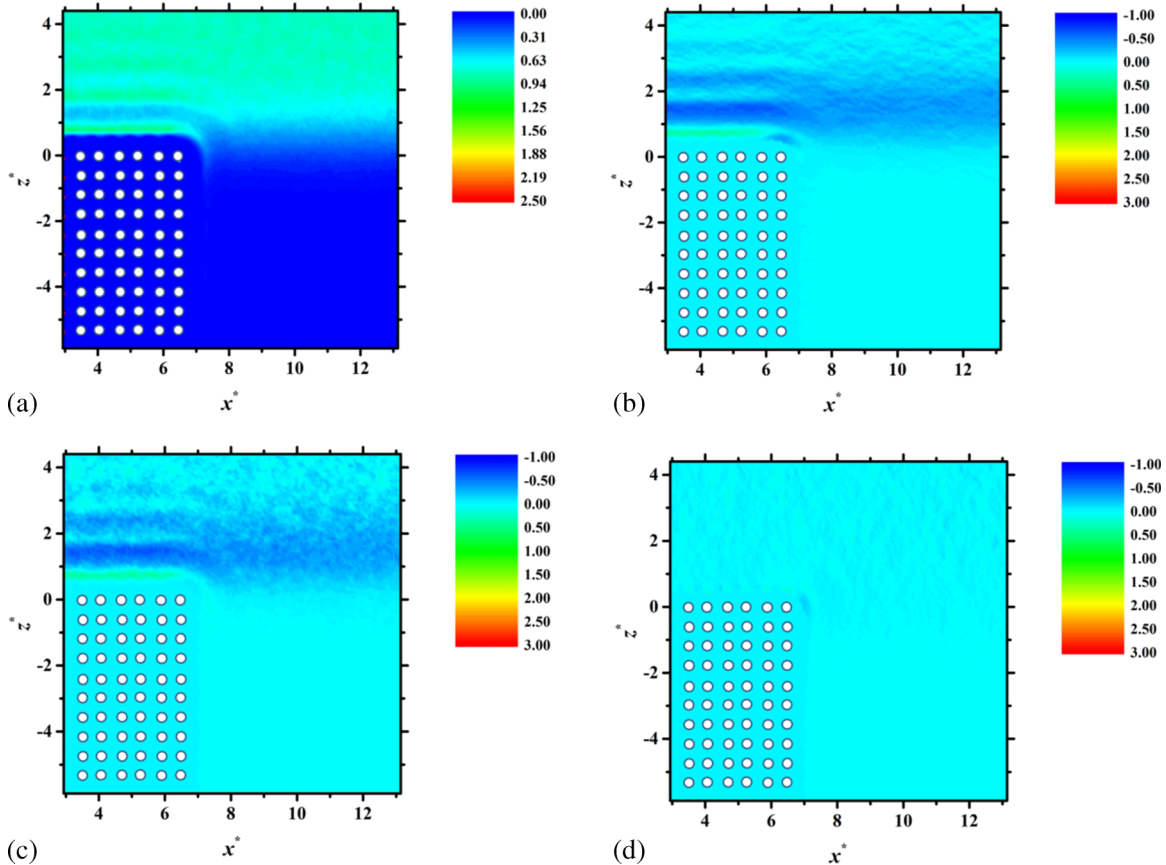


FIG. 3. Reduced density and pressure components of the fluid in the x - z plane for $\varepsilon_{fs} = 0.20$: (a) ρ^* , (b) $\langle \hat{P}_{xx}^* \rangle$, (c) $\langle \hat{P}_{yy}^* \rangle$, and (d) $\langle \hat{P}_{zz}^* \rangle$.

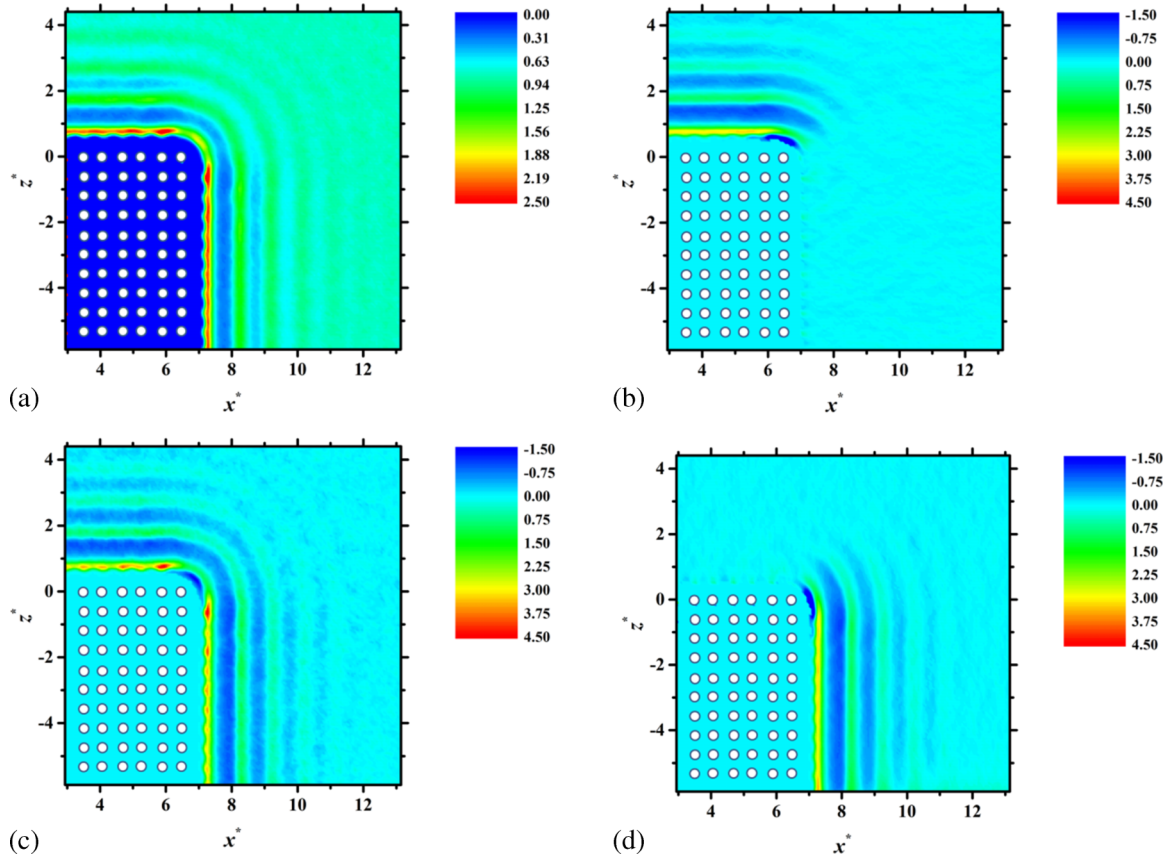


FIG. 4. Reduced density and pressure components of the fluid in the x - z plane for $\varepsilon_{fs} = 0.50$: (a) ρ^* , (b) $\langle \hat{P}_{xx}^* \rangle$, (c) $\langle \hat{P}_{yy}^* \rangle$, and (d) $\langle \hat{P}_{zz}^* \rangle$.

again by the velocity scaling for 500 000 time steps. After these pre-relaxation calculations, the relaxation calculation is conducted for 1 500 000 time steps without the velocity scaling control. The reduced density of the bulk part of the liquid film is 0.793 in equilibrium. The main results of the density, pressure components, and interfacial tension are obtained as the time averaged values for at least 2 000 000 time steps.

IV. RESULTS AND DISCUSSIONS

The results are presented in this section as follows. First, in Sec. IV A, distributions of the density and pressure components of the fluid at the liquid-solid interface with a slit pore are shown in a two dimensional plane, for the two states of the liquid film: (a) liquid film on the slit and (b) liquid film in the slit. Section IV B reveals effects of the fluid-solid interaction intensity on the states of the liquid film in the vicinity of the slit, and the relationship between the interfacial tensions obtained outside the slit and the two states are discussed. Finally, local interfacial tensions are obtained in the vicinity of the corner of the slit, and relationships between the local interfacial tensions and the transition mechanism of the two states are discussed in Sec. IV C.

A. Density and pressure components of the fluid at a liquid-solid interface with a slit pore

The distributions of the density and pressure components in the vicinity of the left entrance of the slit are obtained on

the basis of Eq. (3), for each subsystem with the area $A_k (=dx_k \times dz_k = 0.073 \times 0.073)$ in the x - z plane. The results are obtained as the time averaged values of 2 000 000 steps after the relaxation calculation. Figure 3 presents the reduced density ρ^* (Fig. 3(a)) and pressure components: $\langle \hat{P}_{xx}^* \rangle$ (Fig. 3(b)), $\langle \hat{P}_{yy}^* \rangle$ (Fig. 3(c)), and $\langle \hat{P}_{zz}^* \rangle$ (Fig. 3(d)), of the liquid film on the slit pore for $\varepsilon_{fs} = 0.20$. In Figs. 3(a)-3(d), the solid atoms of the left side of the slit are shown as the white circles. Figure 3(a) shows the vapor-liquid interface in the vicinity of the slit is situated above the slit for the relatively weak fluid-solid interaction intensity ($\varepsilon_{fs} = 0.20$). Figures 3(b) and 3(c) confirm that the variation of the pressure components tangential to the liquid-solid interface is significant and the distribution of the pressure components: $\langle \hat{P}_{xx}^* \rangle$ and $\langle \hat{P}_{yy}^* \rangle$ are almost the same. $\langle \hat{P}_{zz}^* \rangle$ in Fig. 3(d) represents no significant distribution, because it is not the component tangential to the liquid-solid interface outside the slit. On the other hand, Figure 4 presents the reduced density distribution (Fig. 4(a)) and pressure components: $\langle \hat{P}_{xx}^* \rangle$ (Fig. 4(b)), $\langle \hat{P}_{yy}^* \rangle$ (Fig. 4(c)), and $\langle \hat{P}_{zz}^* \rangle$ (Fig. 4(d)), of the liquid film in the slit pore for $\varepsilon_{fs} = 0.50$. As is evident from Fig. 4(a), the inside of the slit pore is filled with liquid molecules under the influence of the strong fluid-solid interaction intensity ($\varepsilon_{fs} = 0.50$). The same tendency is observed in Figs. 4(b)-4(d) in that the variations of the pressure components tangential to the liquid-solid interface are significant, and it should also be noted that $\langle \hat{P}_{yy}^* \rangle$ has two observable liquid-solid interfaces because the y direction is normal to the x - z plane. The pressure component $\langle \hat{P}_{zz}^* \rangle$ in Fig. 4(d) has a characteristic profile at the liquid-solid interface inside and outside the slit, corresponding

to the density distribution in Fig. 4(a), and it shows the two highest values in the vicinity of the 2nd solid layer from the corner at both the inside and outside the slit. This suggests that the local pressure components tangential to the solid surface, $\langle \hat{P}_{xx}^* \rangle$ and $\langle \hat{P}_{yy}^* \rangle$, in the vicinity of the 1st fluid layer from the solid surface, are different in a two dimensional plane for a relatively strong fluid-solid interaction intensity ($\epsilon_{fs} = 0.50$), and the difference becomes pronounced in the vicinity of the corner of the slit.

B. Effects of the fluid-solid interaction intensity on the states of the liquid film in the vicinity of the slit

As described in Sec. I, the fluid-solid interaction is one of the dominant factors that determine the two states of the liquid film in the vicinity of the slit; therefore, in this Sec. IV B, effects of the fluid-solid interaction intensity on the states of the liquid film in the vicinity of the slit are examined based on the density, pressure, and interfacial tensions of the fluid. Figure 5 shows the time evolution of the number of fluid molecules in the slit after the relaxation calculation for $\epsilon_{fs} = 0.20-0.50$. The number of the fluid molecules in the slit is defined as the number of the fluid molecules below $z^* = 0.0$ (see Fig. 2(c)). The large number in the cases of $\epsilon_{fs} = 0.43$ and 0.50 indicates that the inside of the slit is filled with fluid molecules, on the other hand, the inside of the slit is not fully filled with the fluid molecules in the cases of $\epsilon_{fs} = 0.20-0.42$, which are the states of the liquid film on the slit. The number

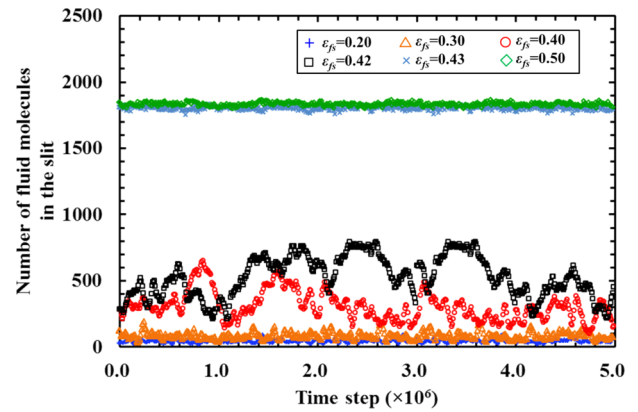


FIG. 5. Time evolution of the number of fluid molecules in the slit for $\epsilon_{fs} = 0.20-0.50$.

of the fluid molecules fluctuates with the passage of time on this time scale, and the fluctuation becomes pronounced with an increase in ϵ_{fs} .

Figures 6(a)-6(d) present reduced density distributions of the fluid molecules in the vicinity of the left corner of the entrance of the slit for $\epsilon_{fs} = 0.30-0.43$. The results are obtained as the averaged values of 2 000 000 time steps. The results show that the liquid film is situated on the slit and partially filling the inside of the slit in the case of $\epsilon_{fs} = 0.40$ and 0.42 (Figs. 6(b) and 6(c)). On increasing the fluid-solid interaction intensity ϵ_{fs} , the local density outside the slit in the vicinity

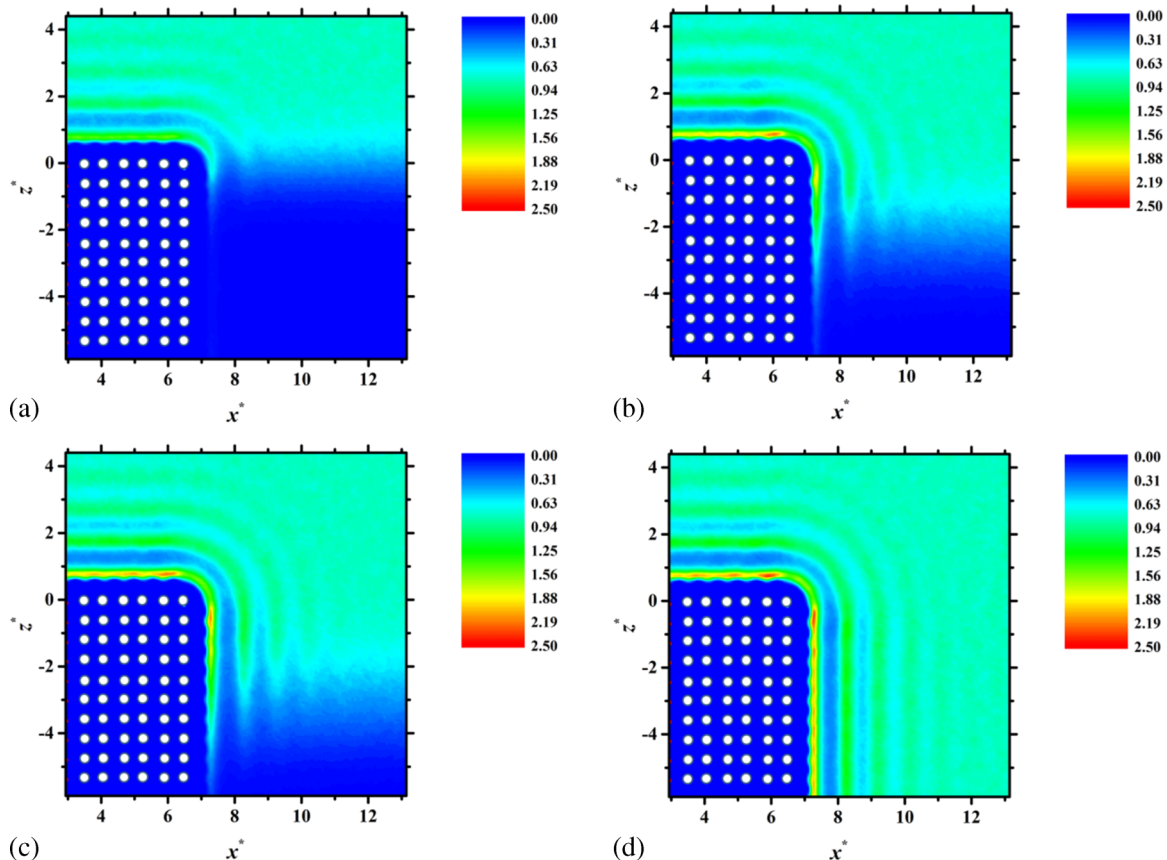


FIG. 6. Reduced density distributions in the x - z plane, of the fluid molecules in the vicinity of the left corner of the entrance of the slit, for various fluid-solid interaction intensities: (a) $\epsilon_{fs} = 0.30$, (b) $\epsilon_{fs} = 0.40$, (c) $\epsilon_{fs} = 0.42$, and (d) $\epsilon_{fs} = 0.43$.

of the corner becomes higher, and with this, the local density inside the slit also becomes higher. The results confirmed that the shape of the vapor-liquid interface is almost flat excluding the layers in the vicinity of the solid surface (Figs. 6(a)-6(c)).

In order to examine the increase of the local density of the fluid in the vicinity of the corner, the reduced density of the fluid molecules, ρ^* , in the x direction at $z^* = 0.77$, where the 1st fluid layer from the solid surface exists outside the slit, is obtained for $\varepsilon_{fs} = 0.20$ -0.43, and the results are presented in Fig. 7. The density profile of the fluid outside the slit in Fig. 7 clearly indicates that the fluid density in the vicinity of the 2nd layer of solid atoms from the corner of the slit becomes higher with an increase in ε_{fs} . It should be added that this tendency is observed also in the two dimensional contour plots in Fig. 4(a), and it affects the value of $\langle \hat{P}_{yy}^* \rangle$ as shown in Fig. 4(c).

The reduced pressure component $\langle \hat{P}_{zz}^* \rangle$ in the vapor region above the liquid film, is calculated to investigate effects of fluid-solid interaction intensity ε_{fs} on the pressure in the system, and the results are given in Fig. 8. The pressure is calculated in the vapor region above the liquid film in the system, defined as the range: $25.0 < z^* < 35.0$, for $\varepsilon_{fs} = 0.20$ -0.50. The result indicates that $\langle \hat{P}_{zz}^* \rangle$ in the vapor region is almost constant, although the vapor-liquid interface in the vicinity of the slit fluctuates with increasing ε_{fs} , as shown in Fig. 5.

In order to clarify the relationship between the interfacial tension and the state of the liquid film on or in the slit, first, reduced local interfacial tensions of the fluid at the liquid-solid interface, $\langle \hat{\gamma}_{z-x}^* \rangle$ and $\langle \hat{\gamma}_{z-y}^* \rangle$, are calculated based on Eq. (4) for $\varepsilon_{fs} = 0.20$ and 0.40, and are shown in Figs. 9(a) and 9(b). The local interfacial tensions are obtained at each local slab, along the z direction, with the height of 0.073: $dz^* = 0.073$, and the values are averaged at the outside of the slit in the range: $0.0 < x^* < 4.7$, where effects of the corner of the slit can be ignored. It can be seen that $\langle \hat{\gamma}_{z-x}^* \rangle$ is identical to $\langle \hat{\gamma}_{z-y}^* \rangle$ for each ε_{fs} , which indicates the space-averaged local liquid-solid interfacial tension is isotropic in the x and y directions at each z position.

From a macroscopic point of view, the slit becomes impregnated with liquid, when the condition below is satisfied in the slit,³⁰

$$I = \gamma_{vs} - \gamma_{ls} > 0, \quad (12)$$

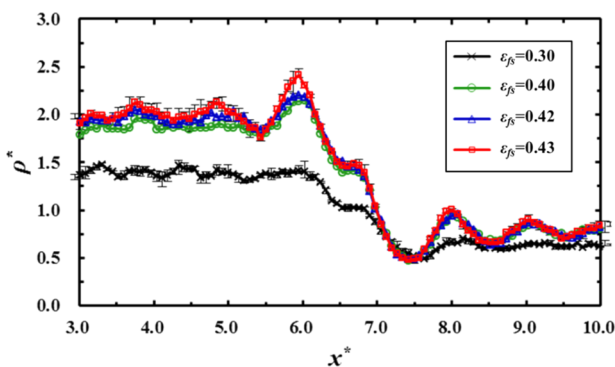


FIG. 7. Reduced density profile of the fluid molecules, ρ^* , in the x direction at $z^* = 0.77$, for $\varepsilon_{fs} = 0.30$ -0.43. The values are obtained as the averaged values of 5 000 000 time steps, and the error bars show the five averaged results of 1 000 000 time steps for $\varepsilon_{fs} = 0.30$ and 0.43.

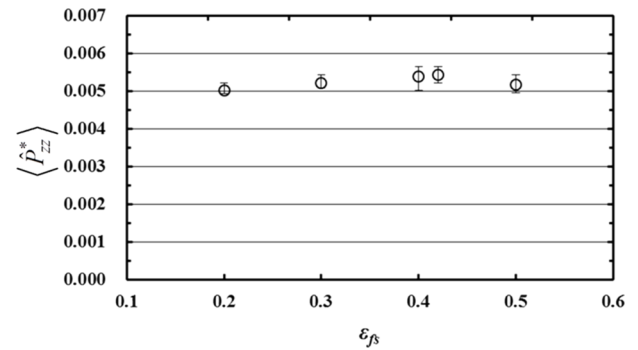


FIG. 8. Reduced pressure component $\langle \hat{P}_{zz}^* \rangle$ in the vapor region above the liquid film in the system for $\varepsilon_{fs} = 0.20, 0.30, 0.40, 0.42, \text{ and } 0.50$. The values of the pressure component are averaged for 5 000 000 time steps, and the error bars show the five averaged results of 1 000 000 time steps. The pressure is calculated in the vapor region above the liquid film in the system, defined as the range: $25.0 < z^* < 35.0$.

where I represents the impregnation parameter and is defined as the difference between the vapor-solid interfacial tension and liquid-solid interfacial tension, $\gamma_{vs} - \gamma_{ls}$. Equation (12) is valid for γ_{vs} and γ_{ls} defined as the values inside the slit, but under the macroscopic condition, the values inside and outside are almost the same for a flat vapor-liquid interfacial system. It suggests that the two states of the liquid film: (a) liquid film on the slit and (b) liquid film in the slit, are predictable from the values of γ_{vs} and γ_{ls} outside the slit. Based on this macroscopic concept, the time-averaged value of the instantaneous

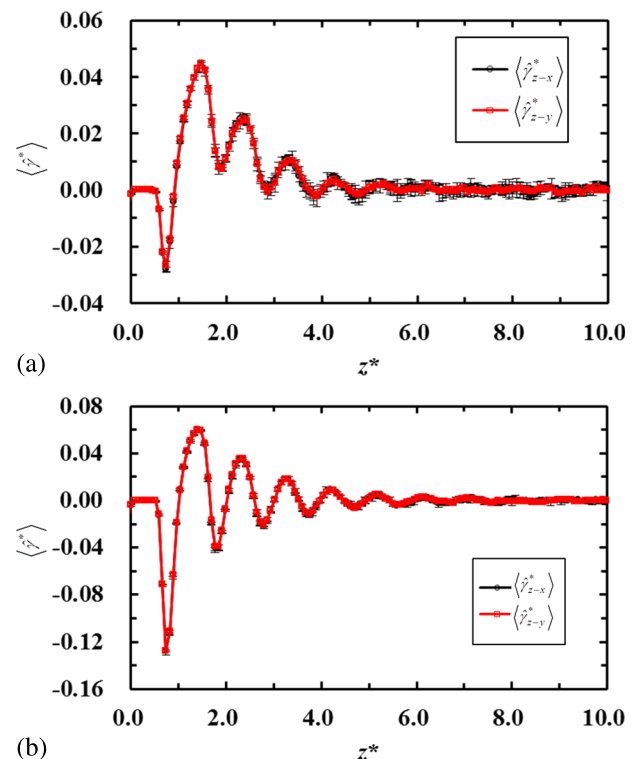


FIG. 9. Reduced interfacial tension, $\langle \hat{\gamma}_{z-x}^* \rangle$ and $\langle \hat{\gamma}_{z-y}^* \rangle$ of the fluid at the liquid-solid interface for (a) $\varepsilon_{fs} = 0.20$ and (b) $\varepsilon_{fs} = 0.40$. The values are obtained in the range: $0.0 < x^* < 4.7$, and are averaged values for 5 000 000 time steps. The error bars are shown by the five averaged results of 1 000 000 time steps.

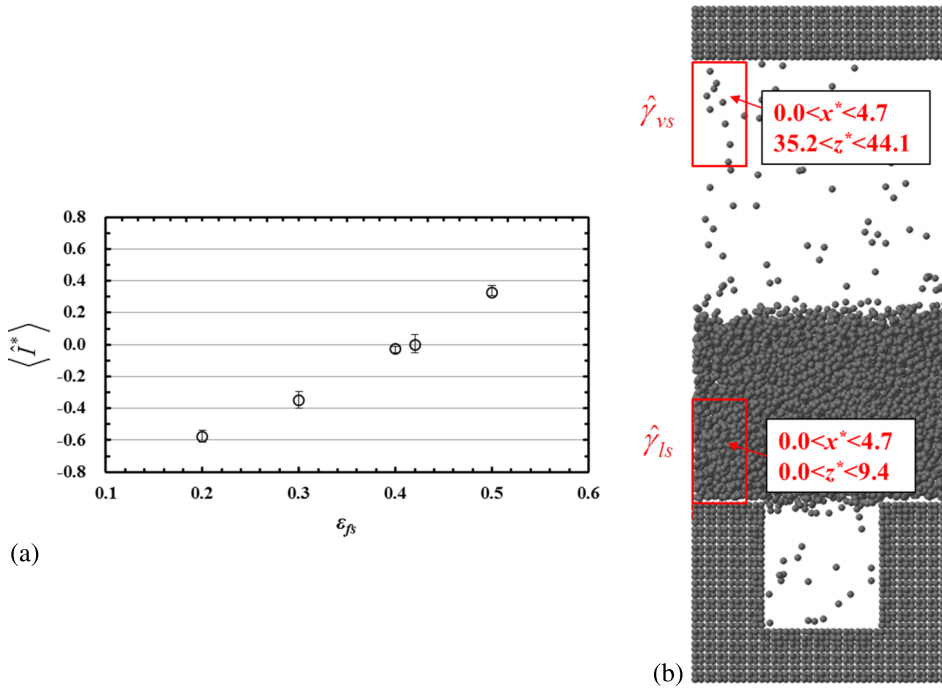


FIG. 10. Effects of the fluid-solid interaction intensities ($\epsilon_{fs} = 0.20-0.50$) on the reduced impregnation parameter $\langle \hat{I}^* \rangle = \langle \hat{\gamma}_{vs}^* \rangle - \langle \hat{\gamma}_{ls}^* \rangle$, and the definition of the area in which $\hat{\gamma}_{vs}$ and $\hat{\gamma}_{ls}$ are calculated. The values of the impregnation parameter are averaged for 5 000 000 time steps, and the error bars are shown by the five averaged results of 1 000 000 steps. (a) Effects of ϵ_{fs} on reduced impregnation parameter, $\langle \hat{I}^* \rangle = \langle \hat{\gamma}_{vs}^* \rangle - \langle \hat{\gamma}_{ls}^* \rangle$. (b) Definition of the calculation area for $\hat{\gamma}_{vs}$ and $\hat{\gamma}_{ls}$.

expression of the impregnation parameter,

$$\langle \hat{I} \rangle = \langle \hat{\gamma}_{vs} \rangle - \langle \hat{\gamma}_{ls} \rangle, \quad (13)$$

which is defined as the values outside the slit, is investigated in the present calculation system, and the reduced results for $\epsilon_{fs} = 0.20-0.50$ are shown in Fig. 10(a). Here, the vapor-solid and liquid-solid interfacial tensions are obtained as the integrated values of the local quantities in the area defined in Fig. 10(b), and are described based on Eq. (5),

$$\begin{aligned} \hat{\gamma}_{vs} &= \int_{\text{Vapor-Solid}} (\hat{P}_{zz, V_k} - \hat{P}_{xx, V_k}) dz_k, \\ \hat{\gamma}_{ls} &= \int_{\text{Liquid-Solid}} (\hat{P}_{zz, V_k} - \hat{P}_{xx, V_k}) dz_k. \end{aligned} \quad (14)$$

Comparing Fig. 10(a) and Fig. 5 reveals that the two states of the liquid film are almost predictable by the time-averaged impregnation parameter obtained from the interfacial tensions outside the slit, but this parameter does not determine a definite threshold between the two states on a molecular time-space

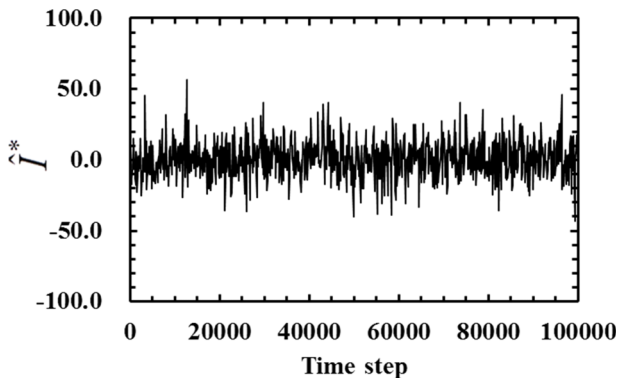


FIG. 11. Time evolution of the instantaneous values of the reduced impregnation parameter: $\hat{I}^* = \hat{\gamma}_{vs}^* - \hat{\gamma}_{ls}^*$. The values of $\hat{\gamma}_{vs}$ and $\hat{\gamma}_{ls}$ are obtained in the area shown in Fig. 10(b) every 100 time steps.

scale, i.e., it does not predict the fluctuations of the liquid film as shown in Fig. 5 and the partially wetted states in Fig. 6. In order to investigate the time dependence of the impregnation parameter, the instantaneous value of the impregnation parameter, \hat{I} is obtained every 100 steps for $\epsilon_{fs} = 0.42$ and the reduced result is shown in Fig. 11. The result shows fluctuations of the value of \hat{I} depending on time, which indicates that the two states of the liquid film cannot be predicted by the instantaneous value of $\langle \hat{I} \rangle$.

C. Transition mechanism between the states of the liquid film based on the local interfacial tensions

In order to reveal in more detail the transition mechanism between the two states of the liquid film: (a) liquid film on the slit and (b) liquid film in the slit, the local interfacial tensions of the fluid in the vicinity of the left entrance of the slit are investigated using Eq. (4). Figure 12 shows the reduced local interfacial tensions $\langle \hat{\gamma}_{x-y}^* \rangle$ and $\langle \hat{\gamma}_{x-z}^* \rangle$ in the $x-z$ plane for $\epsilon_{fs} = 0.42$, where the liquid film is the state before reaching the wetting process as shown in Figs. 5 and 6(c). The results in Fig. 12 show characteristic distributions of $\langle \hat{\gamma}_{x-y}^* \rangle$ and $\langle \hat{\gamma}_{x-z}^* \rangle$ around the corner inside the slit, and reveal a minimum value in the vicinity of the 2nd layer of the solid atoms inside the slit as shown in Fig. 12(a). To investigate the local interfacial tensions in detail, $\langle \hat{\gamma}_{x-y}^* \rangle$ and $\langle \hat{\gamma}_{x-z}^* \rangle$ in the vicinity of the 1st fluid layer from the solid surface inside the slit, along the z direction (at $x^* = 7.30$), are shown in Fig. 13 for $\epsilon_{fs} = 0.40, 0.42, \text{ and } 0.43$, where the inside of the slit is filled with liquid molecules in the case of $\epsilon_{fs} = 0.43$. Figure 13 reveals that there are points where the values of $\langle \hat{\gamma}_{x-y}^* \rangle$ and $\langle \hat{\gamma}_{x-z}^* \rangle$ are locally low (at around $z^* = -0.5$ for $\langle \hat{\gamma}_{x-y}^* \rangle$ and $z^* = -1.0$ for $\langle \hat{\gamma}_{x-z}^* \rangle$), for each value of ϵ_{fs} , and the values in the case of the liquid film on the slit ($\epsilon_{fs} = 0.40$) approach the values of the case that the inside of the slit is filled with the fluid molecules ($\epsilon_{fs} = 0.43$).

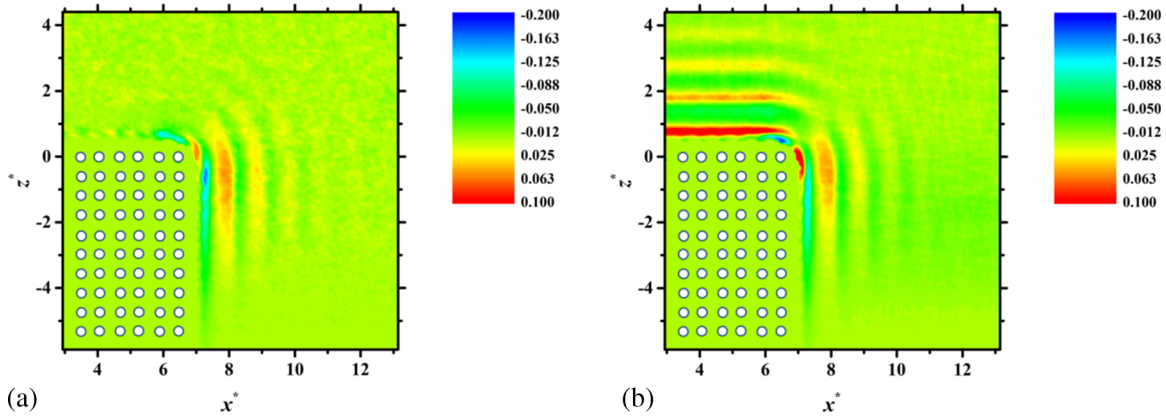


FIG. 12. Reduced local interfacial tensions in the x - z plane in the vicinity of the left corner of the entrance of the slit for $\epsilon_{fs} = 0.42$: (a) $\langle \hat{\gamma}_{x-y}^* \rangle$ and (b) $\langle \hat{\gamma}_{x-z}^* \rangle$. The values are obtained as the averaged values of 2 000 000 time steps.

The minimum value of $\langle \hat{\gamma}_{x-y}^* \rangle$ is lower than that of $\langle \hat{\gamma}_{x-z}^* \rangle$ for each ϵ_{fs} , which corresponds to the density profile of the fluid molecules in the x - z plane in Figs. 6(b)-6(d). It suggests that the local interfacial tensions, $\langle \hat{\gamma}_{x-y}^* \rangle$ at around $z^* = -0.5$: in the vicinity of the 2nd layer of solid atoms inside the slit, and $\langle \hat{\gamma}_{x-z}^* \rangle$ at around $z^* = -1.0$: in the vicinity of the 3rd layer of solid atoms, act as a trigger to cause the transition between the two states. In order to examine the relationships of the local interfacial tensions between inside and outside the slit in the vicinity of the corner, $\langle \hat{\gamma}_{z-x}^* \rangle$ and $\langle \hat{\gamma}_{z-y}^* \rangle$ in the vicinity of the 1st fluid layer from the solid surface outside the slit ($z^* = 0.77$), along the x direction, are shown in Fig. 14 for $\epsilon_{fs} = 0.40, 0.42$, and 0.43 . Here, the local interfacial tensions $\langle \hat{\gamma}_{z-y}^* \rangle$ for each ϵ_{fs} represent locally low values, as is the case for $\langle \hat{\gamma}_{x-y}^* \rangle$ in Fig. 13, and it corresponds to the density profile as shown in Fig. 7. It is also found that the minimum values of $\langle \hat{\gamma}_{z-y}^* \rangle$ for $\epsilon_{fs} = 0.40$ and 0.42 , obtained outside the slit, are lower than those of $\langle \hat{\gamma}_{x-y}^* \rangle$ obtained inside the slit, when the transition between the two states does not occur.

Focusing on the point where $\langle \hat{\gamma}_{x-y}^* \rangle$ is the lowest value along the z direction, in the vicinity of the 2nd layer of the solid atoms inside the slit, the local interfacial tensions $\langle \hat{\gamma}_{x-y}^* \rangle$ and

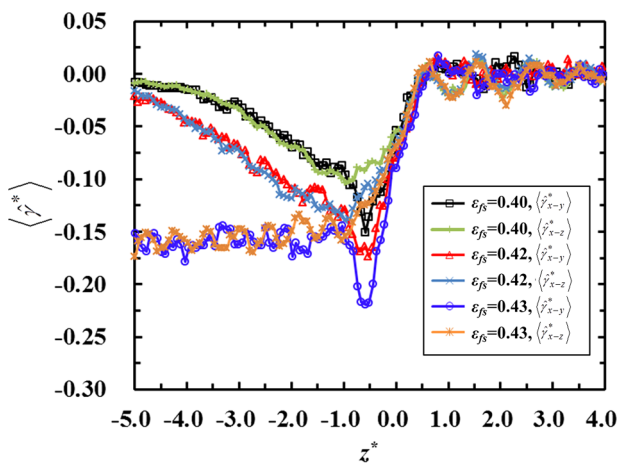


FIG. 13. Reduced local interfacial tensions $\langle \hat{\gamma}_{x-y}^* \rangle$ and $\langle \hat{\gamma}_{x-z}^* \rangle$ along the z direction, in the vicinity of the 1st fluid layer from the solid surface inside the slit ($x^* = 7.30$), for $\epsilon_{fs} = 0.40, 0.42$, and 0.43 . The values are obtained as the averaged values of 2 000 000 time steps.

$\langle \hat{\gamma}_{x-z}^* \rangle$ at $z^* = -0.55$ are calculated along the x direction for $\epsilon_{fs} = 0.42$ and 0.43 , and the results are presented in Fig. 15. It can be seen from Fig. 15 that $\langle \hat{\gamma}_{x-y}^* \rangle$ ($\epsilon_{fs} = 0.42$) almost satisfies the state of $\langle \hat{\gamma}_{x-y}^* \rangle$ ($\epsilon_{fs} = 0.43$) excluding the minimum

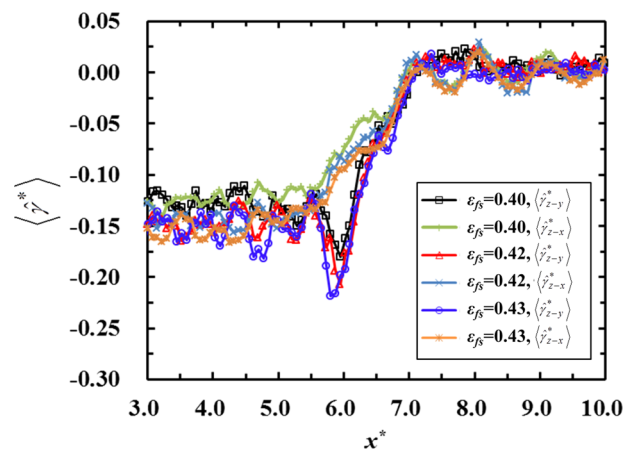


FIG. 14. Reduced local interfacial tensions $\langle \hat{\gamma}_{z-x}^* \rangle$ and $\langle \hat{\gamma}_{z-y}^* \rangle$ along the x direction, in the vicinity of the 1st fluid layer from the solid surface outside the slit ($z^* = 0.77$), for $\epsilon_{fs} = 0.40, 0.42$, and 0.43 . The values are obtained as the averaged values of 2 000 000 time steps.

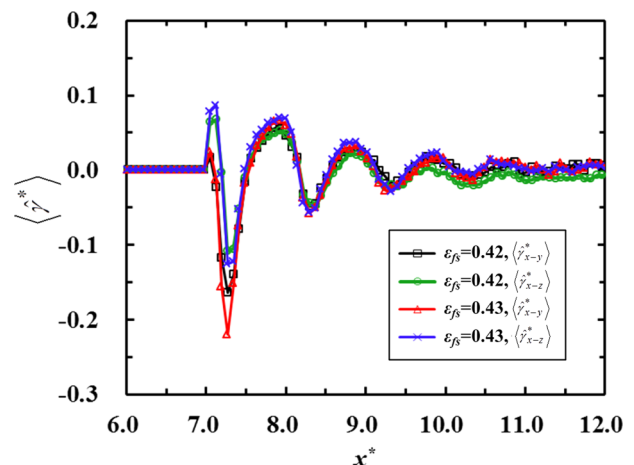


FIG. 15. Reduced local interfacial tensions $\langle \hat{\gamma}_{x-y}^* \rangle$ and $\langle \hat{\gamma}_{x-z}^* \rangle$ along the x direction at $z^* = -0.55$, for $\epsilon_{fs} = 0.42$ and 0.43 . The values are obtained as the averaged values of 2 000 000 time steps.

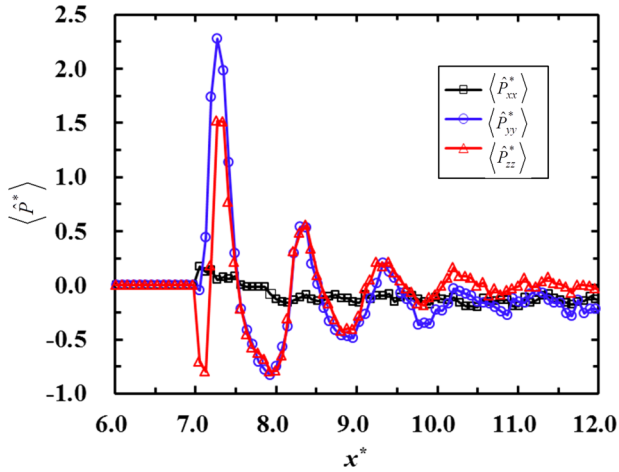


FIG. 16. Reduced pressure components, $\langle \hat{P}_{xx}^* \rangle$, $\langle \hat{P}_{yy}^* \rangle$, and $\langle \hat{P}_{zz}^* \rangle$ along the x direction at $z^* = -0.55$, for $\epsilon_{fs} = 0.42$. The values are obtained as the averaged values of 2 000 000 time steps.

value at $x^* = 7.30$, although $\langle \hat{\gamma}_{x-z}^* \rangle$ ($\epsilon_{fs} = 0.42$) is different from that of $\epsilon_{fs} = 0.43$ at each y position. In particular, it can also be seen that $\langle \hat{\gamma}_{x-z}^* \rangle$ ($\epsilon_{fs} = 0.42$) is lower than 0.0 in the vicinity of the center of the slit ($x^* = 12.0$). In order to investigate $\langle \hat{\gamma}_{x-y}^* \rangle$ and $\langle \hat{\gamma}_{x-z}^* \rangle$ for $\epsilon_{fs} = 0.42$ in detail, the local pressure components, $\langle \hat{P}_{xx}^* \rangle$, $\langle \hat{P}_{yy}^* \rangle$, and $\langle \hat{P}_{zz}^* \rangle$ are obtained by using Eq. (3), and the results are shown in Fig. 16. According to Fig. 16, $\langle \hat{P}_{xx}^* \rangle$ and $\langle \hat{P}_{yy}^* \rangle$ are lower than 0.0 in the vicinity of the center of the slit, due to the effects of the vapor-liquid interface, and that is why $\langle \hat{\gamma}_{x-z}^* \rangle$ ($\epsilon_{fs} = 0.42$) is lower than 0.0 in the vicinity of the center of the slit as seen in Fig. 15. It should be noted that $\langle \hat{P}_{xx}^* \rangle$ is not lower than 0.0 in the vicinity of the 1st layer of fluid molecules from the solid surface, and which means the effect of the low value of $\langle \hat{P}_{xx}^* \rangle$ is weak in the vicinity of the 1st fluid layer from the solid surface.

Figure 17 shows the time evolution of the local interfacial tension $\hat{\gamma}_{x-y}^*$ at $(x^*, z^*) = (7.30, -0.55)$ for $\epsilon_{fs} = 0.42$, where the value of the time-averaged local interfacial tension $\langle \hat{\gamma}_{x-y}^* \rangle$ is the lowest as shown in Fig. 13. In Fig. 17, significant spikes are observed instantaneously, which shows a more pronounced tendency compared with the case of \hat{I}^* in Fig. 11. It is also found in Fig. 17 that the negative spikes are significant compared with the positive spikes, which is the evidence of the negative value of $\langle \hat{\gamma}_{x-y}^* \rangle$ as shown in Fig. 13.

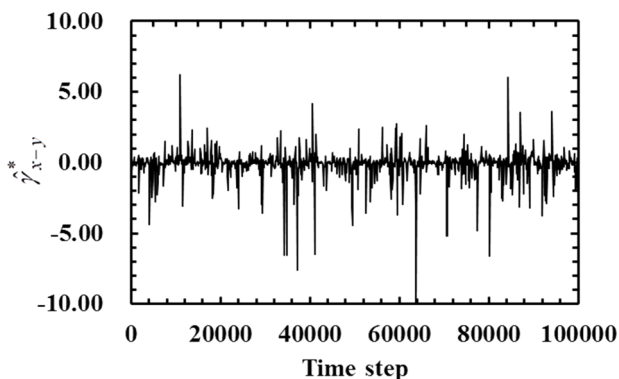


FIG. 17. Time evolution of the local interfacial tension, $\hat{\gamma}_{x-y}^*$ at $(x^*, z^*) = (7.30, -0.55)$, for $\epsilon_{fs} = 0.42$. The value is obtained every 100 time steps.

V. CONCLUSIONS

In this paper, a classical molecular dynamics simulation was conducted for a liquid-solid interfacial system with a nanometer-scale slit pore in order to reveal local thermodynamic states: local pressure components and interfacial tensions of a liquid film in the vicinity of the slit. The simulation was also used to investigate the transition mechanism between the two states of the liquid film: (a) liquid film on the slit and (b) liquid film in the slit, based on the local thermodynamic quantities from a molecular point of view. Based on a volume perturbation, an instantaneous expression of the local pressure components and interfacial tensions was presented to investigate time-dependent phenomena in molecular dynamics simulations. The interactions between the particles were described by the 12-6 Lennard-Jones potential, and effects of the fluid-solid interaction intensity on the local pressure components and interfacial tensions of the liquid film in the vicinity of the slit were examined in detail by this presented perturbative method. The main conclusions obtained in the present study are summarized as follows:

- The results of the time-averaged density distribution of the fluid show that there are states where the liquid film is situated on the slit partially filling the inside of the slit, before reaching the wetting process. Increasing the fluid-solid interaction intensity leads to the local density of the fluid outside the slit in the vicinity of the corner becoming higher, and with this, the local density inside the slit also becomes higher, before reaching the wetting process. The state of the liquid film in the slit has two peaks of the fluid density in the vicinity of the corner of the slit.
- The local pressure components tangential to the solid surface in the vicinity of the 1st fluid layer from the solid surface are different in a two dimensional plane, and the difference becomes pronounced in the vicinity of the corner of the slit, for cases where the fluid-solid interaction intensities are relatively strong.
- The occurrence of the liquid film in one state or the other depends for the most part on the impregnation parameter outside the slit, which is defined as the difference between the integrated vapor-liquid and liquid-solid interfacial tensions acting on the fluid, but it does not determine a definite threshold between the two states on a molecular time-space scale, i.e., it does not predict the fluctuations of the liquid film and the partially wetted states.
- The local interfacial tensions in the vicinity of the 1st fluid layer from the solid surface inside the slit, $\langle \hat{\gamma}_{x-y}^* \rangle$ and $\langle \hat{\gamma}_{x-z}^* \rangle$, which are defined by using the pressure components in the width (x), depth (y), and height (z) directions of the slit, indicate that there are points where the values of $\langle \hat{\gamma}_{x-y}^* \rangle$ and $\langle \hat{\gamma}_{x-z}^* \rangle$ are locally low in the vicinity of the 2nd and 3rd layers of solid atoms from the entrance of the slit, respectively, for each fluid-solid interaction intensity. Furthermore, with an increase in the fluid-solid interaction intensity, the minimum value in the case of the liquid film on the slit, approaches the

value of the case that the inside of the slit is filled with the liquid molecules.

- The minimum value of $\langle \hat{\gamma}_{z-y}^* \rangle$ in the vicinity of the 1st fluid layer from the solid atoms outside the slit is lower than that of $\langle \hat{\gamma}_{x-y}^* \rangle$ obtained inside the slit, for the cases that the liquid film is on the slit. Furthermore, the pressure components along the width (x) direction in the slit, at the minimum value of $\langle \hat{\gamma}_{x-y}^* \rangle$, reveal that the pressure components tangential to a vapor-liquid interface influence the values of $\langle \hat{\gamma}_{x-y}^* \rangle$ and $\langle \hat{\gamma}_{x-z}^* \rangle$ in the vicinity of the center of the slit, but the effect is weak for the minimum values of $\langle \hat{\gamma}_{x-y}^* \rangle$ and $\langle \hat{\gamma}_{x-z}^* \rangle$. We conclude that the local interfacial tensions inside the slit, $\langle \hat{\gamma}_{x-y}^* \rangle$ and $\langle \hat{\gamma}_{x-z}^* \rangle$, in the vicinity of the 2nd and 3rd layers of the solid atoms from the entrance of the slit, respectively, act as a trigger to cause the transition between the two states of the liquid film.

These results suggest that there exist the phenomena on a molecular temporal-spatial scale which are not comprehended through the thermodynamic quantities based on the macroscopic concept, and which lead to the transport of condensed matters. The results also indicate that the local fluid density in the vicinity of the solid surface influences on the local thermodynamic quantities. Therefore, even for a complicated system, in which polar interactions are considered, this transition mechanism could be applicable if the variation of the fluid density is observed in the vicinity of the corner of the slit.

ACKNOWLEDGMENTS

The authors are grateful to Dr. M. Arita, Dr. S. Nadahara, Mr. K. Terashima, Mr. K. Kinose, Mr. T. Funayoshi, Mr. Y. Nakazawa, Mr. I. Kajino, Mr. T. Kawamura, and Mr. J. Yoshida of SCREEN Holdings Co., Ltd. for supporting this work.

APPENDIX A: RELATIONSHIP BETWEEN THE EQUATION IN EQUILIBRIUM AND INSTANTANEOUS EXPRESSION

The relationship between the established equation applicable in equilibrium and the instantaneous expression (Eq. (3)) is shown as follows. First, based on the established equation applicable in equilibrium,²⁴ the $\xi\xi$ component of the local pressure is described as

$$P_{\xi\xi, V_k} = \frac{1}{\beta \Delta(d\xi_k) A_{\xi, V_k}} \times \ln \left(\left(1 + \frac{\Delta V_k}{V_k} \right)^{N_{V_k}} \exp(-\beta \Delta(U_{V_k} + \Phi_{V_k})) \right), \quad (\text{A1})$$

where β is defined as $\beta = 1/(k_B T)$ with the Boltzmann constant k_B and the absolute temperature T , N_{V_k} is the number of fluid molecules in the local volume V_k , and $\langle \rangle$ represents the ensemble average. In an equilibrium state, the relationship below is assumed to be satisfied,³¹

$$\frac{3}{2} N_{V_k} k_B \hat{T}_{V_k} = \sum_{i \in V_k} \frac{1}{2} \frac{|\mathbf{p}_i|^2}{m_i}, \quad (\text{A2})$$

where \hat{T}_{V_k} denotes the instantaneous temperature in V_k , and its time-averaged value is equal to the temperature in V_k : $T_{V_k} = \langle \hat{T}_{V_k} \rangle$. Equation (A2) assumes the isotropic states below,

$$\begin{aligned} \frac{1}{2} N_{V_k} k_B \hat{T}_{V_k} &= \sum_{i \in V_k} \frac{1}{2} \frac{p_{ix}^2}{m_i}, \\ \frac{1}{2} N_{V_k} k_B \hat{T}_{V_k} &= \sum_{i \in V_k} \frac{1}{2} \frac{p_{iy}^2}{m_i}, \\ \frac{1}{2} N_{V_k} k_B \hat{T}_{V_k} &= \sum_{i \in V_k} \frac{1}{2} \frac{p_{iz}^2}{m_i}. \end{aligned} \quad (\text{A3})$$

Under this assumption, the time-averaged expression of Eq. (3) becomes

$$\begin{aligned} \langle \hat{P}_{\xi\xi, V_k} \rangle &= \left\langle \frac{1}{\Delta(d\xi_k) A_{\xi, V_k}} \left[\sum_{i \in V_k} \frac{p_{i\xi}^2 \Delta V_k}{m_i V_k} - \Delta(U_{V_k} + \Phi_{V_k}) \right] \right\rangle \\ &= \frac{1}{\Delta(d\xi_k) A_{\xi, V_k}} \left\langle N_{V_k} k_B \hat{T}_{V_k} \ln \left(1 + \frac{\Delta V_k}{V_k} \right) + k_B \hat{T}_{V_k} \ln \left[\exp \left(-\frac{\Delta(U_{V_k} + \Phi_{V_k})}{k_B \hat{T}_{V_k}} \right) \right] \right\rangle \\ &= \frac{k_B}{\Delta(d\xi_k) A_{\xi, V_k}} \left\langle \hat{T}_{V_k} \ln \left[\left(1 + \frac{\Delta V_k}{V_k} \right)^{N_{V_k}} \exp \left(-\frac{\Delta(U_{V_k} + \Phi_{V_k})}{k_B \hat{T}_{V_k}} \right) \right] \right\rangle \\ &\cong \frac{1}{\beta \Delta(d\xi_k) A_{\xi, V_k}} \left\langle \ln \left[\left(1 + \frac{\Delta V_k}{V_k} \right)^{N_{V_k}} \exp(-\beta \Delta(U_{V_k} + \Phi_{V_k})) \right] \right\rangle, \end{aligned} \quad (\text{A4})$$

where we used the approximation: $\ln(1 + \Delta V_k/V_k) \approx \Delta V_k/V_k$ for the case of $1 \gg \Delta V_k/V_k$. The final form in Eq. (A4) is approximately obtained by using the relationship of $T = \langle \hat{T}_{V_k} \rangle$ after a long time average. Eq. (A4) is similar to Eq. (A1), but the bracket in Eq. (A4) includes “ln,” which avoids the time average of the Boltzmann factor in the molecular dynamics simulation.

APPENDIX B: METHOD TO EVALUATE THE LOCAL ENERGY

A method to evaluate the energy difference in the local volume is presented in this Appendix B. Consider a situation shown in Fig. 18(a), where the i th and j th particles are

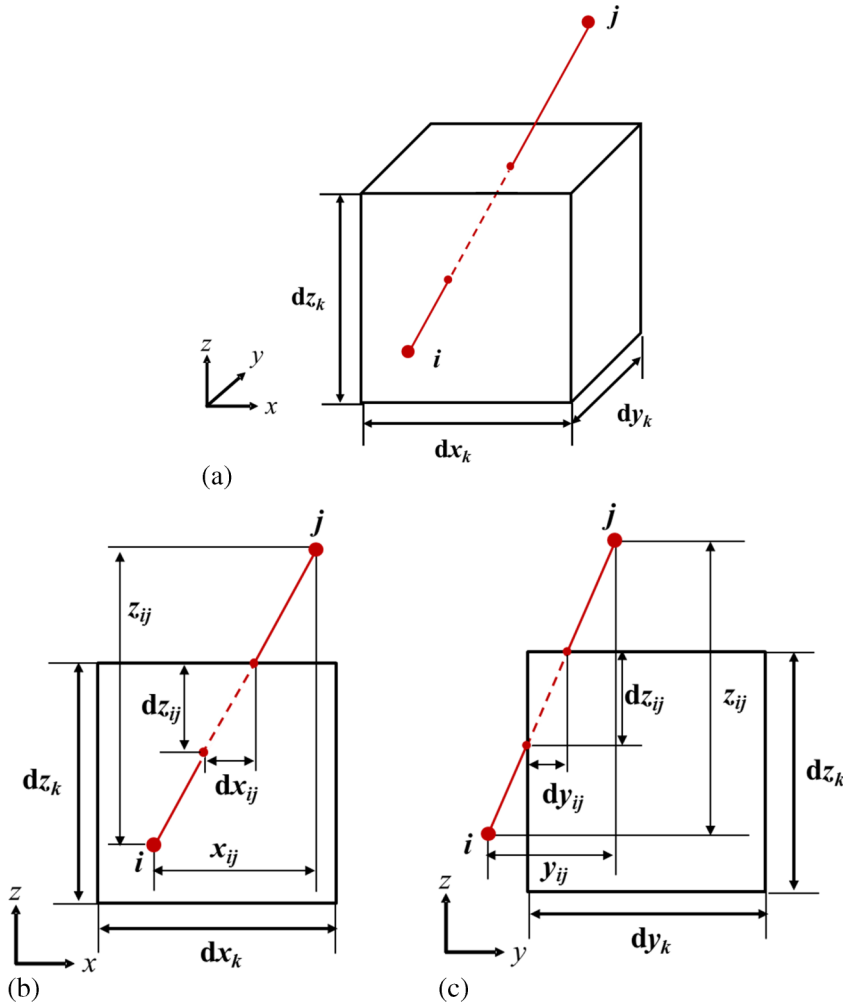


FIG. 18. Definition of the line segment between the i th and j th particles inside and outside a local volume. (a) The i th and j th particles interacting through a local volume. (b) View from the y direction. (c) View from the x direction.

interacting with each other through a local volume V_k . In Fig. 18(a), the part of the line segment between the positions of the i th and j th particles is inside the volume. The part inside the volume is evaluated by the variation of the local volume. For instance, to obtain the local pressure component \hat{P}_{zz,V_k} , the evaluation of the energy difference by the local volume perturbation in the z direction is needed. In reference to Figs. 18(b) and 18(c), the potential energy in the local volume in the initial state, U_{0,V_k} , due to the interaction between the i th and j th particles, is

$$U_{0,V_k} = U_{0,V_k}(r_{ij,0}) \times \frac{dz_{ij,0}}{z_{ij,0}}. \quad (B1)$$

On the other hand, the potential energy in the perturbed local volume, U_{1,V_k} , is

$$U_{1,V_k} = U_{1,V_k}(r_{ij,1}) \times \frac{dz_{ij,1}}{z_{ij,1}}. \quad (B2)$$

Then, the energy difference is evaluated as below,

$$\begin{aligned} \Delta U_{V_k} &= U_{1,V_k} - U_{0V_k} \\ &= (U_{1,V_k}(r_{ij,1}) - U_{0,V_k}(r_{ij,0})) \times \frac{dz_{ij,0}}{z_{ij,0}}. \end{aligned} \quad (B3)$$

In Eq. (B3), the relationships: $z_{ij,1} = (1 + \lambda)z_{ij,0}$ and $dz_{ij,1} = (1 + \lambda)dz_{ij,0}$ are considered. The other components of the pressure are evaluated in the same manner.

APPENDIX C: DISCUSSION ON THE VALIDATION OF THE LOCAL QUANTITIES

In the present study, the local quantities: density, pressure components, and interfacial tensions, are calculated at a small volume $V_k (= dx_k \times dy_k \times dz_k = 0.073 \times 17.76 \times 0.073 \approx 0.095)$ where the side of the area $A_k (= dx_k \times dz_k = 0.073 \times 0.073)$ in the x - z plane is less than a molecular diameter. This Appendix C is devoted to discuss the validation of the quantities calculated at such a small volume.

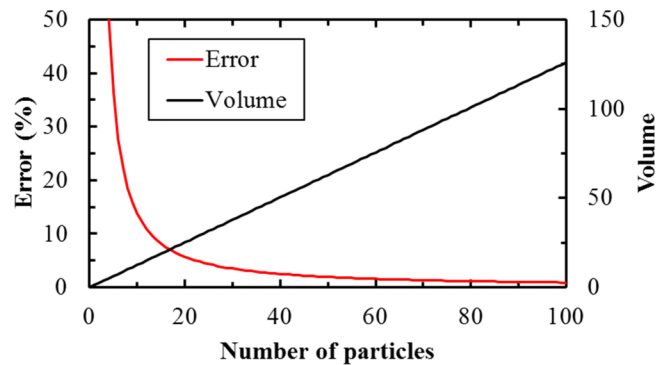


FIG. 19. The error between $\ln(n!)$ and $(n \ln(n) - n)$, and the size of the volume, for the variation of the number of particles. The error is defined as $|\ln(n!) - (n \ln(n) - n)| / \ln(n!)$, and the size of the volume is calculated by using the value of the bulk density of the liquid film on the slit pore ($= 0.793$).

In Appendix A, we showed the relationship between the equation in equilibrium (Eq. (A1)) and the instantaneous expression (Eq. (3)); however, from a rigorous theoretical point of view, it is valid for the case that each subsystem contains a large number of particles. In equilibrium statistical mechanics, the partition function is defined at each subsystem under the condition that each subsystem is independent: the volume of each subsystem is large enough to ignore effects of the molecular interactions at the boundary of the volume. Let us estimate the appropriate size of the volume based on the validation of the Stirling's approximation ($\ln(n!) \approx n\ln(n) - n$) which is a premise for the existence of the partition function. Figure 19 shows the error between $\ln(n!)$ and $(n\ln(n) - n)$, and the size of the volume, for the variation of the number of particles. The size of the volume is calculated by using the value of the bulk density of the liquid film on the slit pore ($=0.793$). For example, if the approximation is valid with an uncertainty of 1.0%, approximately 90 particles are needed to be contained in the volume. In that case, the size of the cube is 113.5 (each side is 4.842), which is 1199 times larger than the local volume adopted in this study. It is to be remarked that this is a rough estimation, and more particles are needed for the case where the Stirling's approximation is used more precisely. Therefore, based on this result, Eq. (3) should be used for subsystems which have such large volumes from a theoretical point of view. Ibergay *et al.*²² calculated local quantities in one dimension by the perturbative method for a vapor-liquid interfacial system, and investigated local spatial correlation functions defined between the local volumes by molecular simulations. As a result, they showed that the local quantities are uncorrelated. We respect their approach as a numerical check; however, this does not meet the exact definition of subsystems because the decorrelation does not ensure the independence between the subsystems. In this study, our standpoint is that the quantities calculated at the local volumes are parts which consist of a thermodynamic quantity, and they can be obtained numerically by the method described in Appendix B. We call such quantities local thermodynamic quantities. It should be noted that even if there is no particle instantaneously in the local volume, the local quantities can be obtained by contributions of the intermolecular forces based on Eq. (3) and the method in Appendix B. The values of the local

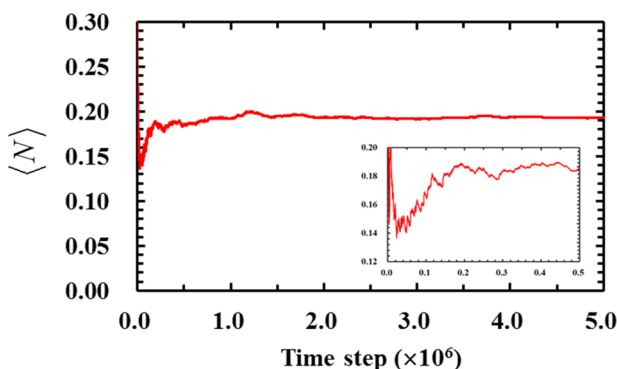


FIG. 20. The time-averaged number of the fluid particles in the local volume at each time step for $\epsilon_{fs} = 0.42$. The location of the local volume is at $(x^*, z^*) = (7.30, -0.55)$.

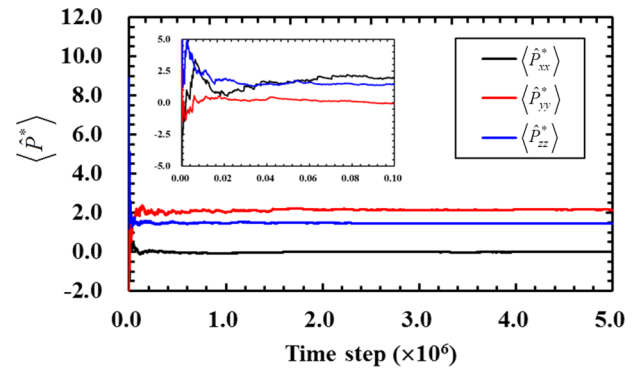


FIG. 21. Effects of the number of the time steps on the time-averaged pressure components $\langle \hat{P}_{xx}^* \rangle$, $\langle \hat{P}_{yy}^* \rangle$, and $\langle \hat{P}_{zz}^* \rangle$ at the local volume for $\epsilon_{fs} = 0.42$. The location of the local volume is at $(x^*, z^*) = (7.30, -0.55)$.

quantities are meaningful if they are constant by averaging the configurations of the particles. We present some results for the validation by numerically showing effects of the number of the time steps on the local quantities.

Figure 20 shows the time-averaged number of the fluid particles in the local volume at each time step for $\epsilon_{fs} = 0.42$. The location of the local volume is the same as that in Fig. 17: $(x^*, z^*) = (7.30, -0.55)$, where the local interfacial tension represents the locally low value. The result reveals that the time-averaged value converges to a constant value (≈ 0.2) at approximately 2 000 000 time steps, where the value of 0.2 indicates that the number of the fluid particles in the local volume is less than one particle as the averaged value. However, the result also reveals that the long-time average allows us to obtain numerically reliable quantity even at such a small volume. Figure 21 presents results of the pressure components, $\langle \hat{P}_{xx}^* \rangle$, $\langle \hat{P}_{yy}^* \rangle$, and $\langle \hat{P}_{zz}^* \rangle$ at the local volume, where the values are obtained by the time averaging at each time step for $\epsilon_{fs} = 0.42$. The time-averaged local pressure components fluctuate significantly in the range of the short time-average ($< 0.1 \times 10^6$), but each value converges by being averaged for a long time. In addition, the interfacial tensions at the local volume, $\langle \hat{\gamma}_{x-y}^* \rangle$ and $\langle \hat{\gamma}_{x-z}^* \rangle$ are obtained at each time step as the time-averaged values for $\epsilon_{fs} = 0.42$, and the results are given in Fig. 22. The results confirm that the local interfacial tensions also converge by the long-time average. As shown in Figs. 20-22, the local quantities calculated in this

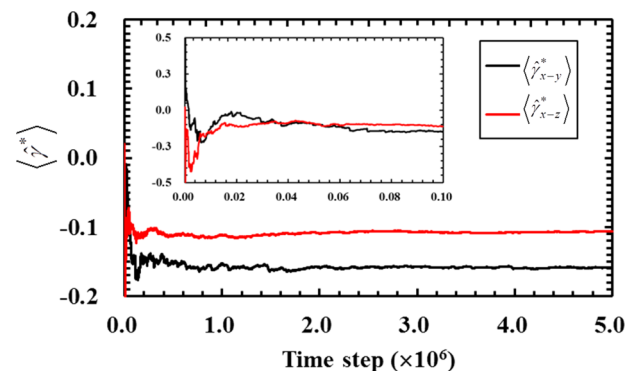


FIG. 22. Effects of the number of the time steps on the time-averaged interfacial tensions, $\langle \hat{\gamma}_{x-y}^* \rangle$ and $\langle \hat{\gamma}_{x-z}^* \rangle$ at the local volume for $\epsilon_{fs} = 0.42$. The location of the local volume is at $(x^*, z^*) = (7.30, -0.55)$.

study can be obtained numerically as the reliable values by the long-time average in the molecular dynamics simulation.

- ¹J. L. Plawsky, A. G. Fedorov, S. V. Garimella, H. B. Ma, S. C. Maroo, L. Chen, and Y. Nam, *Nanoscale Microscale Thermophys. Eng.* **18**, 251 (2014).
- ²R. B. Schoch, J. Han, and P. Renaud, *Rev. Mod. Phys.* **80**, 839 (2008).
- ³T. Ito, T. Yamada, Y. Inao, T. Yamaguchi, N. Mizutani, and R. Kuroda, *Appl. Phys. Lett.* **89**, 033113 (2006).
- ⁴G. M. Choi, *Solid State Phenom.* **219**, 3 (2014).
- ⁵A. B. D. Cassie and S. Baxter, *Trans. Faraday Soc.* **40**, 546 (1944).
- ⁶R. N. Wenzel, *Ind. Eng. Chem.* **28**, 988 (1936).
- ⁷S. S. Latthe, A. B. Gurav, C. S. Maruti, and R. S. Vhatkar, *J. Surf. Eng. Mater. Adv. Technol.* **2**, 76 (2012).
- ⁸P. Roach, N. J. Shirtcliffe, and M. I. Newton, *Soft Matter* **4**, 224 (2008).
- ⁹N. Verplanck, Y. Coffinier, V. Thomy, and R. Boukherroub, *Nanoscale Res. Lett.* **2**, 577 (2007).
- ¹⁰B. Shi and V. K. Dhir, *J. Chem. Phys.* **130**, 034705 (2009).
- ¹¹F. Ould-Kaddour and D. Levesque, *J. Chem. Phys.* **135**, 224705 (2011).
- ¹²K. Fujiwara and M. Shibahara, *Nanoscale Microscale Thermophys. Eng.* **17**, 1 (2013).
- ¹³T. Koishi, K. Yasuoka, S. Fujikawa, T. Ebisuzaki, and X. C. Zeng, *Proc. Natl. Acad. Sci. U.S.A.* **106**, 8435 (2009).
- ¹⁴S. Chen, J. Wang, T. Ma, and D. Chen, *J. Chem. Phys.* **140**, 114704 (2014).
- ¹⁵A. Shahraz, A. Borhan, and K. A. Fichtorn, *Langmuir* **29**, 11632 (2013).
- ¹⁶J. H. Irving and J. G. Kirkwood, *J. Chem. Phys.* **18**, 817 (1950).
- ¹⁷B. D. Todd, D. J. Evans, and P. J. Daivis, *Phys. Rev. E* **52**, 1627 (1995).
- ¹⁸J.-P. Hansen and I. R. McDonald, *Theory of Simple Liquids*, 4th ed. (Academic, Oxford, 2013).
- ¹⁹E. de Miguel and G. Jackson, *J. Chem. Phys.* **125**, 164109 (2006).
- ²⁰A. Ghoufi and P. Malfreyt, *J. Chem. Phys.* **135**, 104105 (2011).
- ²¹A. Ghoufi and P. Malfreyt, *J. Chem. Phys.* **136**, 024104 (2012).
- ²²C. Ibergay, A. Ghoufi, F. Goujon, P. Ungerer, A. Boutin, B. Rousseau, and P. Malfreyt, *Phys. Rev. E* **75**, 051602 (2007).
- ²³G. J. Gloor, G. Jackson, F. J. Blas, and E. de Miguel, *J. Chem. Phys.* **123**, 134703 (2005).
- ²⁴K. Fujiwara and M. Shibahara, *J. Chem. Phys.* **141**, 034707 (2014).
- ²⁵J. S. Rowlinson and B. Widom, *Molecular Theory of Capillarity* (Clarendon, Oxford, 1982).
- ²⁶M. J. P. Nijmeijer, C. Bruin, A. F. Bakker, and J. M. J. van Leeuwen, *Phys. Rev. A* **42**, 6052 (1990).
- ²⁷S. Zhu and M. R. Philpott, *J. Chem. Phys.* **100**, 6961 (1994).
- ²⁸J. C. Tully, *J. Chem. Phys.* **73**, 1975 (1980).
- ²⁹S. Maruyama, *Adv. Numer. Heat Transfer* **2**, 189 (2000).
- ³⁰P. G. de Gennes, F. Brochard-Wyart, and D. Quéré, *Capillarity and Wetting Phenomena: Drops, Bubbles, Pearls, Waves* (Springer, New York, 2004).
- ³¹D. J. Evans and G. Morriss, *Statistical Mechanics of Nonequilibrium Liquids*, 2nd ed. (Cambridge University, Cambridge, 2008).